Influence of nickel substrate grain structure on $YBa_2Cu_3O_{7-x}$ supercurrent connectivity in deformation-textured coated conductors

D. M. Feldmann, J. L. Reeves, A. A. Polyanskii, G. Kozlowski, R. R. Biggers,[a] R. M. Nekkanti,[a] I. Maartense,[a] M. Tomsic,[b] P. Barnes,[a] C. E. Oberly,[a] T. L. Peterson,[a] S. E. Babcock, and D. C. Larbalestier[c]
Applied Superconductivity Center, University of Wisconsin–Madison, Madison, Wisconsin 53706

(Received 9 June 2000; accepted for publication 14 August 2000)

Coupled magneto-optical imaging and local misorientation angle mapping have been used to demonstrate the percolative nature of supercurrent flow in $YBa_2Cu_3O_{7-x}$(YBCO) coated conductors grown on deformation-textured Ni substrates. Barriers to current flow occur at many YBCO grain boundaries (GBs) which have propagated through the buffer layers from the underlying Ni substrate, and all Ni GBs with misorientation angles $>4°$ initiate percolative current flow. This type of current barrier is characteristic of the conductor form and has been found to exist in samples with J_c(0 T,77 K) values >2 MA/cm^2. Sharpening of the local substrate texture or improving in low-angle GB properties should lead to higher J_c values. © *2000 American Institute of Physics.* [S0003-6951(00)00341-7]

High critical current density (J_c) conductors capable of operating in fields of several tesla at liquid-nitrogen temperature are critical to large-scale applications of high-temperature superconductors. Coated conductors (CCs) with biaxially textured $YBa_2Cu_3O_x$(YBCO) respond to this need.[1–3] One widely employed approach today uses deformation texturing of a metal substrate, generally pure Ni, on which buffer layers and YBCO are grown.[1,2] Such architectures permit J_c(0 T,77 K) values[1,2] >1 MA/cm^2, but many samples have lower values. Here we couple magneto-optical imaging and local misorientation angle mapping to show that many such barriers to current flow occur at YBCO grain boundaries (GBs) which have propagated through the buffer layers from the Ni GBs in the underlying substrate. All Ni GBs with misorientation angles $>4°$ were found to initiate percolative current flow. Since typical deformation-textured substrates have many GBs misoriented in the range of 5°–10°, this study shows that it will be very valuable for CC technology to further enhance substrate texture and/or to improve low-angle GB properties.

Magneto-optical (MO) imaging, light microscopy, and backscattered electron Kikuchi pattern (BEKP) analysis of the local texture were conducted on a series of four CC samples grown on deformation-textured Ni substratres with in-plane and out-of-plane full width at half maxima of 6.6°–7.4° and 5.8°–8.7°, respectively, as measured by x-ray pole figures. The buffer and YBCO layers were deposited by pulsed-laser deposition (PLD) with architecture YBCO/CeO_2/yttria-stabilized zirconia (YSZ)/CeO_2/Ni and thickness of 300–1200/100/500/100 nm for the respective oxide layers. The thickness of the YBCO layer varied from sample to sample without obvious differences in the properties measured by MO imaging and ac susceptibility. A 0.6-μm-thick YBCO sample had a high transport J_c(0 T,77 K) of 1.2 MA/cm^2. The remaining samples were taken directly to other characterizations.

A representative MO image of the granular flux-penetration network obtained using standard imaging procedures[4,5] is shown in Fig. 1. This network is common to CCs with varying constructions from multiple sources. Among the variations are deformation-textured substrates from two different sources and buffer layer combinations, which include CeO_2, YSZ, Y_2O_3,[6] and Eu_2O_3,[7] deposited by e-beam, sputtering, PLD, and sol–gel[7] techniques. YBCO deposition methods included PLD, BaF_2,[1] and trifluoroacetate (TFA).[2] Every one of more than two dozen CCs of the above-mentioned different combinations with J_c(0 T,77 K) values from 0.1 to 2.4 MA/cm^2 was found to exhibit qualitatively similar electromagnetic granularity.[8] The pattern and average separation ($\sim$100 μm) of the bright lines in the MO image, which map flux penetration, are characteristic of the grain structure of the underlying Ni substrate. An example of this granular flux network is shown at higher magnification in Fig. 2(a). Light microscopy of the surface of the YBCO [Fig. 2(b)] shows a grain structure which correlates well to the MO image. Some, but not all, of the GBs of Fig. 2(b) can be immediately matched up to the flux-penetration network of Fig. 2(a). To verify the suspected source of this granularity, the sample was chemically etched to expose the underlying Ni substrate. A light micrograph of the Ni surface is presented in Fig. 2(c). Figure 2(d) overlays the MO and Ni images, making it clear that flux penetration in the YBCO does occur preferentially above Ni GBs, but that not all Ni GBs provoke flux entry. The montage of Fig. 2 shows conclusively that important features of the underlying Ni grain structure directly replicate themselves in the subsequently deposited YBCO layer.

Earlier studies of flux penetration in YBCO bicrystals[4,9] have shown that GBs become visible in MO images when the *inter*granular current density J_{cb} is smaller than the *intra*granular current density J_{cg}. In thin-film [001] tilt bicrys-

[a]Air Force Research Laboratory, Wright–Patterson Air Force Base, OH 45433.
[b]Eurus–Plastronic Technologies Inc., Tallahassee, FL 43210.
[c]Electronic mail: larbales@engr.wisc.edu

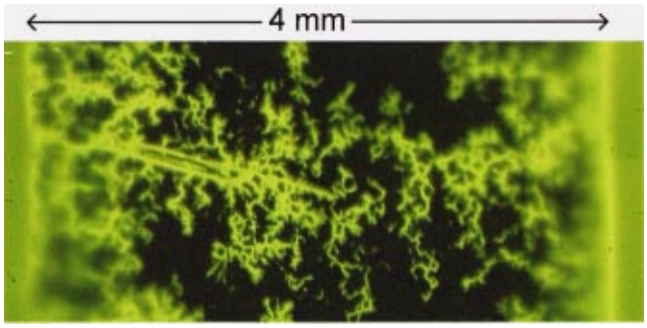

FIG. 1. (Color) MO image taken across the whole width of a 4×10 mm coated conductor after cooling in zero field to 15 K and then applying a field of 60 mT. Bright areas indicate magnetic flux penetration, dark areas flux shielding. Magnetic flux enters the sample from the edges and propagates preferentially along weaker-linked regions such as grain boundaries. The two straight-line defects at the left derive from scratches present on the substrate before film growth. YBCO thickness is 0.6 μm.

tals we have found general agreement between the MO imaging and the transport J_{cb} and J_{cg} results,[4,10] which also show good general agreement with other well-known transport studies.[11,12] Since the magnitude of flux penetration at a GB increases as J_{cb}/J_{cg} decreases,[4] qualitative comparisons of the current-carrying capability of the GBs are possible. Accordingly, we estimated the relative magnitude of flux penetration by measuring the MO image intensity at more than 60 of the GBs in Fig. 2, comparing this intensity to the misorientation angle (θ) measured using BEKP analysis. Figure 3 shows a marked threshold at 4°: flux does not penetrate

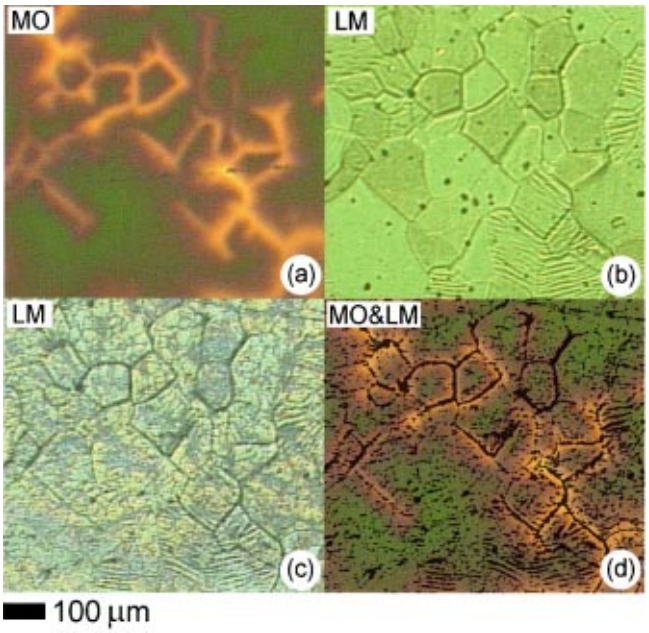

FIG. 2. (Color) MO and light microscopy images of the same location, demonstrating the influence of grain boundaries in the Ni substrate on the flux-penetration pattern and on the visible YBCO GB structure. (a) MO image of a 1.2-μm-thick YBCO sample. The sample was cooled in 60 mT from above T_c to 50 K, and then the field was removed. Darker (green) areas are electromagnetically well-connected regions, while the lighter (orange) flux network indicates where the local current density is reduced (b) Light micrograph of the surface of the YBCO, showing a visible GB structure similar to the MO image. (c) Light micrograph of the underlying Ni substrate after the buffer layers were etched away. Etching was done with a 2:3 mixture of NH_4F(40%) and HF(48%). (d) Overlay of (a) and (c) showing that flux penetration occurs almost exclusively along Ni grain boundaries and also that not all Ni grain boundaries admit flux.

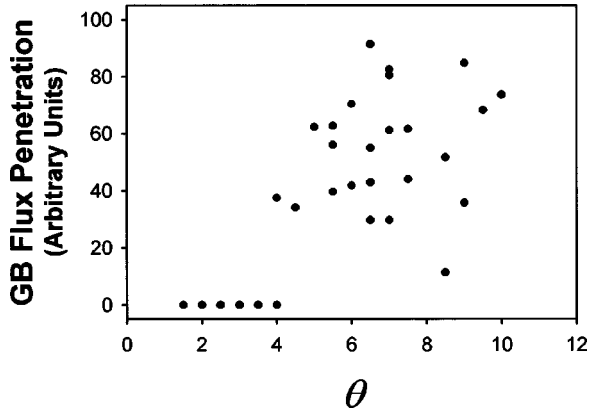

FIG. 3. Intensity of flux penetration vs GB misorientation angle as determined by BEKP analysis from more than 60 grain boundaries in Fig. 2. The flux intensity was determined by averaging the pixel intensity along the boundary. The pixel intensity scales directly with the magnetic field.

above Ni GBs with $\theta<4°$, while boundaries with $\theta>4°$ do exhibit MO contrast. It can also be seen that the magnitude of flux penetration for $\theta>4°$ varies considerably and not very systematically with θ, suggesting that other variables start to control the GB properties at larger θ.

The direct correlation between θ and flux penetration is given in Fig. 4. Figure 4(a) is a *percolation map*, in which a grain is defined as a set of points for which each point has a neighbor that has the same crystallographic orientation, in this case to within 1°. Each grain on the map is shaded a different color. Similarly, Fig. 4(b) is a percolation map for

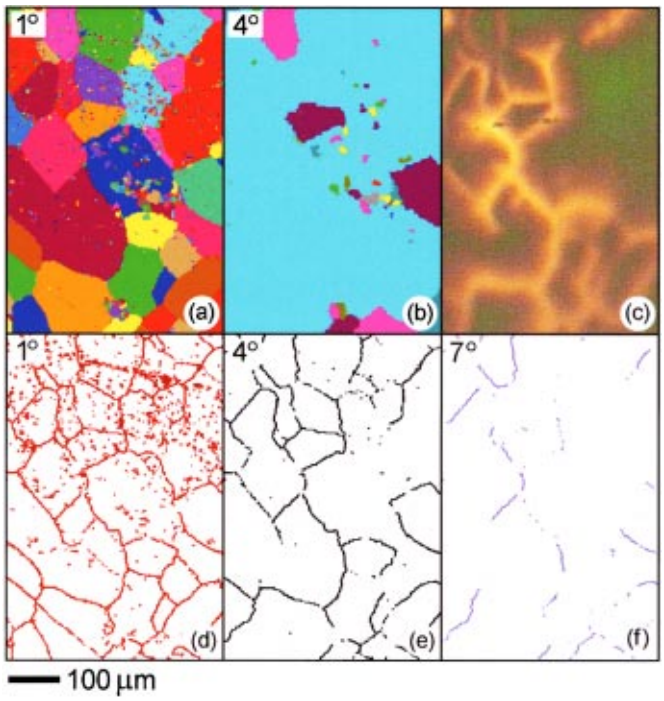

FIG. 4. (Color) MO image and corresponding BEKP maps. The data was taken on a 3 μm grid over a roughly 500×500 μm area. (a) BEKP data presented in the form of a percolation map in which all points are colored the same if there is a continuous connection having point-to-point misorientations of $\leqslant1°$. (b) BEKP percolation map of the same region as (a), but for a point-to-point misorientation criterion of 4°. (c) MO image of the same region of the sample. (d)–(f) Grain-boundary maps of the location of all boundaries for which θ is $\geqslant1°$, 4°, and 7°, respectively. The 4° boundary map in (e) most strongly resembles the MO image.

which the crystal orientation criterion is 4°. This 4° percolation map might suggest that the sample is single-crystal-like with respect to current flow, a conclusion that is at variance with the MO image. Figure 4(e) is a *grain-boundary map*, which shows the location of all grain boundaries for which θ is $>4°$. A comparison of the $\theta>4°$ GB map [Fig. 4(e)], the $\theta=4°$ percolation map [Fig. 4(b)], and the MO image [Fig. 4(c)] shows that many current barriers introduced by Ni GBs with $\theta>4°$ are absent from the percolation map. In fact, there is an almost one-to-one correlation between the location of boundaries with $\theta>4°$ and the flux penetration network. In other words, *percolation maps* show when there is a continuous path through the microstructure for a given grain misorientation criterion, while *grain-boundary maps* more accurately show the cross section available to current at a given θ. Figures 4(d)–4(f) show the evolution of the GB map with increasing minimum θ value. The $\theta>7°$ map in Fig. 4(f) shows many fewer GBs than the $\theta>4°$ map, and the $\theta>10°$ map (not shown) is almost featureless.

The montage of Fig. 4 focuses attention on the factors that control the misorientation angle at which low-angle GBs become barriers to current. Several studies suggest that this is in the vicinity of 7° for [001] tilt YBCO bicrystals,[9–11,13] though some studies[11,14] have also seen strongly depressed properties in some samples at or below 5°. The marked threshold seen here at $\theta=4°$ is qualitatively consistent with these bicrystal data, but it is of concern that the threshold angle is somewhat smaller. Whether this is because the misorientations of coated conductors are not pure [001] tilt, whether because the YBCO boundaries are more grooved, or whether because their *intra*granular current densities are higher (perhaps due to a greater defect density[13,15]) is not yet clear. All such factors can determine the threshold angle, as well as being likely causes of the scatter above 4° seen in Fig. 3. The presence of a sharp threshold and a comparison of the GB maps of Figs. 4(d)–4(f) immediately suggest two important goals for process improvement. One is to improve the *local* texture of the substrate, while a second is to engineer the threshold angle to greater values, an approach suggested possible by the results of Heinig *et al.*[10] and by recent studies of Ca doping of $YBa_2Cu_3O_x$ thin films.[16,17]

An important goal of the much present scale-up is to achieve $J_c>2$ MA/cm^2 in 1–2 μm-thick films.[18,19] A recent analysis of flux flow in bicrystals suggests that the J_c of coated conductors will always be dominated by weak, multiply connected channels such as the flux-penetration network imaged here.[20] Also, the nonlinear voltage–current characteristics of superconductors[21] produce strongly enhanced local dissipation near barriers to current flow. Thus, the coupling of magneto-optical and local orientation imaging to directly reveal the percolative nature of supercurrent flow in CC samples provides a vital insight for the technology, as it matures towards longer lengths, nonmagnetic substrates, thicker YBCO layers, and more automated processes. The percolative current flow occurs in samples with $J_c(0\ \mathrm{T},77\ \mathrm{K})$ values exceeding 1 MA/cm^2 is a direct proof of the significant untapped potential of the coated conductor. Characterizations such as the present can reveal how to realize this potential.

The authors thank E. Hellstrom for advice on etching oxides and they are grateful to A. Ichinose (CRIEPI) and C. Y. Yang for discussions of their coated conductor work. The authors also thank their colleagues at the American Superconductor Corporation, Los Alamos National Laboratory and Oak Ridge National Laboratory who have supplied them with samples for this study. This work was supported by AFOSR, DOE, EPRI, and the NSF-funded MRSEC on Nanostructured Materials.

[1] A. Goyal, S. X. Ren, E. D. Specht, D. M. Kroeger, R. Feenstra, D. Norton, M. Paranthaman, D. F. Lee, and D. K. Christen, Micron **30**, 563 (1999).
[2] A. P. Malozemoff, S. Annavarapu, L. Fritzemeier, Q. Li, V. Prunier, M. Rupich, C. Thieme, and W. Zhang, Inst. Phys. Conf. Ser. **167**, 167 (2000).
[3] S. R. Foltyn, P. N. Arendt, P. C. Dowden, R. F. DePaula, J. R. Groves, J. Y. Coulter, Q. Jia, M. P. Maley, and D. E. Peterson, IEEE Trans. Appl. Supercond. **9**, 1519 (1999).
[4] A. A. Polyanskii, A. Gurevich, A. E. Pashitski, N. F. Heinig, R. D. Redwing, J. E. Nordman, and D. C. Larbalestier, Phys. Rev. B **53**, 8687 (1996).
[5] A. E. Pashitski, A. Gurevich, A. A. Polyanskii, D. C. Larbalestier, A. Goyal, E. D. Specht, D. M. Kroeger, J. A. DeLuca, and J. E. Tkaczyk, Science **275**, 367 (1997).
[6] A. Ichinose, C. Y. Yang, D. C. Larbalestier, S. E. Babcock, A. Kikuchi, K. Tachikawa, and S. Akita, Physica C **324**, 113 (1999).
[7] M. Paranthaman, R. Feenstra, D. F. Lee, D. B. Beash, J. S. Morrell, T. G. Chirayil, A. Goyal, X. Cui, D. T. Verebelyi, J. E. Mathis, P. M. Martin, D. P. Norton, E. D. Specht, D. K. Christen, and D. M. Kroeger, Adv. Cryog. Eng. (in press).
[8] D. M. Feldmann, A. A. Polyanskii, and D. C. Larbalestier (unpublished work). We have imaged more than two dozen deformation textured samples with $J_c(0\ \mathrm{T},77\ \mathrm{K})$ values from 0.1 to 2.4 MA/cm^2 and all of them exhibit qualitatively similar granular structure. There is a positive correlation between higher J_c and reduced granularity.
[9] M. Turchinskaya, D. L. Kaiser, F. W. Gayle, A. J. Shapiro, A. Roytburd, L. A. Dorosinskii, V. I. Nikitenko, A. A. Polyanskii, and V. K. Vlasko-Vlasov, Physica C **221**, 62 (1994).
[10] N. F. Heinig, R. D. Redwing, J. E. Nordman, and D. C. Larbalestier, Phys. Rev. B **60**, 1409 (1999).
[11] D. Dimos, P. Chaudhari, and J. Mannhart, Phys. Rev. B **41**, 4038 (1990).
[12] Z. G. Ivanov, P. A. Nilsson, D. Winkler, J. A. Alarco, T. Claeson, E. A. Stepantsov, and A. Y. Tzalenchuk, Appl. Phys. Lett. **59**, 3030 (1991).
[13] D. Verebelyi, C. Prouteau, R. Feenstra, and D. Christen, IEEE Trans. Appl. Supercond. **9**, 2655 (1999).
[14] D. T. Verebelyi, D. K. Christen, R. Feenstra, C. Cantoni, A. Goyal, D. F. Lee, P. N. Arendt, R. F. DePaula, R. J. Groves, and C. Prouteau, Appl. Phys. Lett. **76**, 1755 (2000).
[15] A. Diaz, L. Mechin, P. Berghuis, and J. E. Evetts, Phys. Rev. Lett. **80**, 3855 (1998).
[16] A. Schmehl, B. Goetz, R. R. Schulz, C. W. Schneider, H. Bielefeldt, H. Hilgenkamp, and J. Mannhart, Europhys. Lett. **47**, 110 (1999); G. Hammerl, A. Schmehl, R. R. Schulz, B. Goetz, H. Bielefeldt, C. W. Schneider, H. Hilgenkamp, and J. Mannhart, Nature (London) (in press).
[17] G. Daniels, A. Gurevich, and D. C. Larbalestier, Appl. Phys. Lett. (in press).
[18] B. Dam, J. M. Huijbregtse, F. C. Klaassen, R. C. F. van der Geest, G. Doornbos, J. H. Rector, A. M. Testa, S. Freisem, J. C. Martinez, B. Stauble-Pumpin, and R. Griessen, Nature (London) **399**, 439 (1999).
[19] S. R. Foltyn, Q. X. Jia, P. N. Arendt, L. Kinder, Y. Fan, and J. F. Smith, Appl. Phys. Lett. **75**, 3692 (1999).
[20] J. E. Evetts, M. J. Hogg, B. A. Glowacki, N. A. Rutter, and V. N. Tsaneva, Supercond. Sci. Technol. **12**, 1050 (1999).
[21] A. Gurevich and J. McDonald, Phys. Rev. Lett. **81**, 2546 (1998); A. Gurevich and M. Friesen, Phys. Rev. B **62**, 4004 (2000).